"Complex Microfluidic Systems Architectures and Applications to Micropower Generation"
AFOSR grant FA9550-08-1-0345

Integrated Fluidics,
Santa Barbara, CA 93101

July 2008 to December 2009.

Abstract

Many highly efficient complex systems exhibit an architecture that contains a trade-off between reliability of components and the size of the system built up from such components. We advanced a novel microfluidic concept, named μfCPU, the Microfluidic Central Processing Unit, where the key microfluidic operations are performed within a single enclosure, using active, software-based inputs rather than physical hardware changes. Parallelization of such a unit avoids necessity of multiple pumps and valves, reducing the footprint of the device. Use of such devices in parallelized architectures requires a study of reliability of individual components. In this project, we advanced such a study of trade-offs between reliability and parallelization in architectures for microfluidic power generation, optimization of which can lead to revolutionary changes in power density of such devices. On the single device side, we performed an experiment that utilized the concept of synthetic turbulence generation that can resolve the inefficiency of the single device operation. We studied the tradeoff between robustness and size of the system indicated above. We utilized the single-component prior uncertainty estimate based on experiments to simulate parallel architectures consisting of microscale units assembled into a power generator. Our study indicates that micropower generation devices can be substantially improved by using 1) the Synthetic Turbulence Generator to reduce the lenghtscale of mixing in the microcombustor 2) a linear array architecture utilizing several microcombustors, to improve robustness and the stability margin of microcombustion [3]. The tradeoff that we studied is common for a large class of Complex Systems Architectures where reliability of components is traded against the size of the system.

REPORT DOCUMENTATION PAGE

Form Approved
OMB No. 0704-0188

PLEASE DO NOT RETURN YOUR FORM TO THE ABOVE ORGANIZATION.

1. REPORT DATE *(DD-MM-YYYY)*	2. REPORT TYPE	3. DATES COVERED *(From - To)*
07-07-2010	Final Technical	07/01/2008 - 12/31/2009

4. TITLE AND SUBTITLE
Complex Microfluidic Systems Architectures and Applications to Micropower Generation

5a. CONTRACT NUMBER

5b. GRANT NUMBER
FA9550-08-1-0345

5c. PROGRAM ELEMENT NUMBER

6. AUTHOR(S)
Igor Mezic

5d. PROJECT NUMBER

5e. TASK NUMBER

5f. WORK UNIT NUMBER

7. PERFORMING ORGANIZATION NAME(S) AND ADDRESS(ES)
Integrated Fluidics
5276 HOLLISTER AVE
SUITE 159
SANTA BARBARA, CA

8. PERFORMING ORGANIZATION REPORT NUMBER

9. SPONSORING/MONITORING AGENCY NAME(S) AND ADDRESS(ES)
Air Force Office of Scientific Research
875 N Randolph St
Arlington, VA 22203

10. SPONSOR/MONITOR'S ACRONYM(S)

11. SPONSOR/MONITOR'S REPORT NUMBER(S)

12. DISTRIBUTION/AVAILABILITY STATEMENT
Distribution A

13. SUPPLEMENTARY NOTES

14. ABSTRACT

Many highly efficient complex systems exhibit an architecture that contains a trade-off between reliability of components and the size of the system built up from such components. We advanced a novel micro fluidic concept, named mu-fCPU, the Micro fluidic Central Processing Unit, where the key microfluidic operations are performed within a single enclosure, using active, software-based inputs rather than physical hardware changes. Parallelization of such a unit avoids necessity of multiple pumps and valves, reducing the footprint of the device. Use of such devices in parallelized architectures requires a study of reliability of individual components. In this project, we advanced such a study of trade-offs between reliability and parallelization in architectures for microfluidic power generation, optimization of which can lead to revolutionary changes in power density of such devices.

15. SUBJECT TERMS

16. SECURITY CLASSIFICATION OF:			17. LIMITATION OF ABSTRACT	18. NUMBER OF PAGES	19a. NAME OF RESPONSIBLE PERSON
a. REPORT	b. ABSTRACT	c. THIS PAGE			Fariba Fahroo
UU	UU	UU	SAR	12	19b. TELEPHONE NUMBER *(Include area code)* 7036968429

Reset

1 Accomplishments

The key research achievements of the project have been:

1.1 Development of a Synthetic Turbulence Generator Platform and Mixing Experiments

In this section we describe the development of the Synthetic Turbulence Generator - a device that can reduce mixing lengthscale in microcombustion - and the experimental stage and set-up that we used to test it. The basic device design is shown in figure 1. All the lengthscales are given in μm. The main channel extending from left to right has 1mm width. There are two supply channels on the left entering the main channel. These manifolds bring in air and another gas used for flow visualization or combustion. Visible in the figure are also four side channels. These are used for zero-mass flow perturbation of the main channel [2, 1] described further in section 1.1. Such zero-mass flow perturbation at high frequency causes stream in the main channel to laminate and mix.

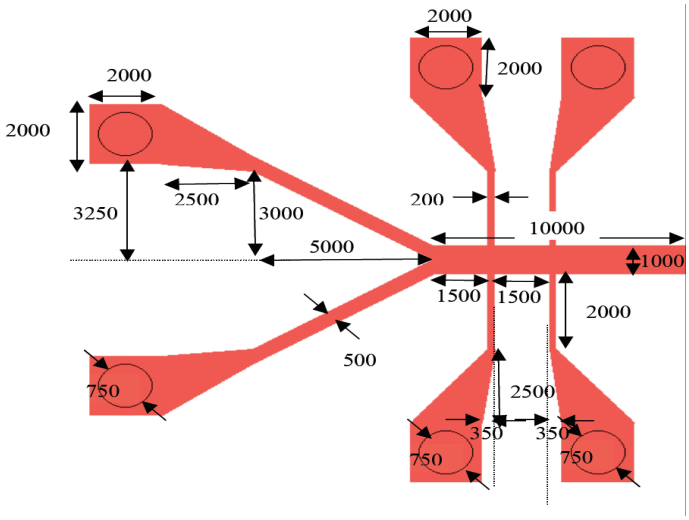

Figure 1: Design of the Synthetic Turbulence Generator

In figure 2 we show the design of the stage (on the right) and the experimental set-up (on the left) for the experiments we performed. The stage was produced out of steel. The experimental set up shown schematically on the left of figure 2 consists of the stage to which inlet manifolds are connected, the STG sitting on the top of the stage, side actuators that are used to induce high-frequency, zero-mass perturbation to the gas flow in the main channel and function generator into which actuation signals can be programmed. The generated waveform is sent through an amplifier inducing actuator action. The side actuators at every side channel consist of an electromagnetic motor connected to the inlet manifold of the side channel by a steel needle. The motion of a steel needle inside the plastic

tubing connected to the side channel via the circular holes shown on the stage schematic on the right of figure 2 induces the translational motion of gas in that side channel and perturbs the main channel flow inducing mixing in the process. A multimeter and Tektronix TDS 3012 oscilloscope are used for measurement purposes. Visual measurement is performed using Nikon Eclipse FN1 epifluorescent microscope on which a high-speed camera is mounted.

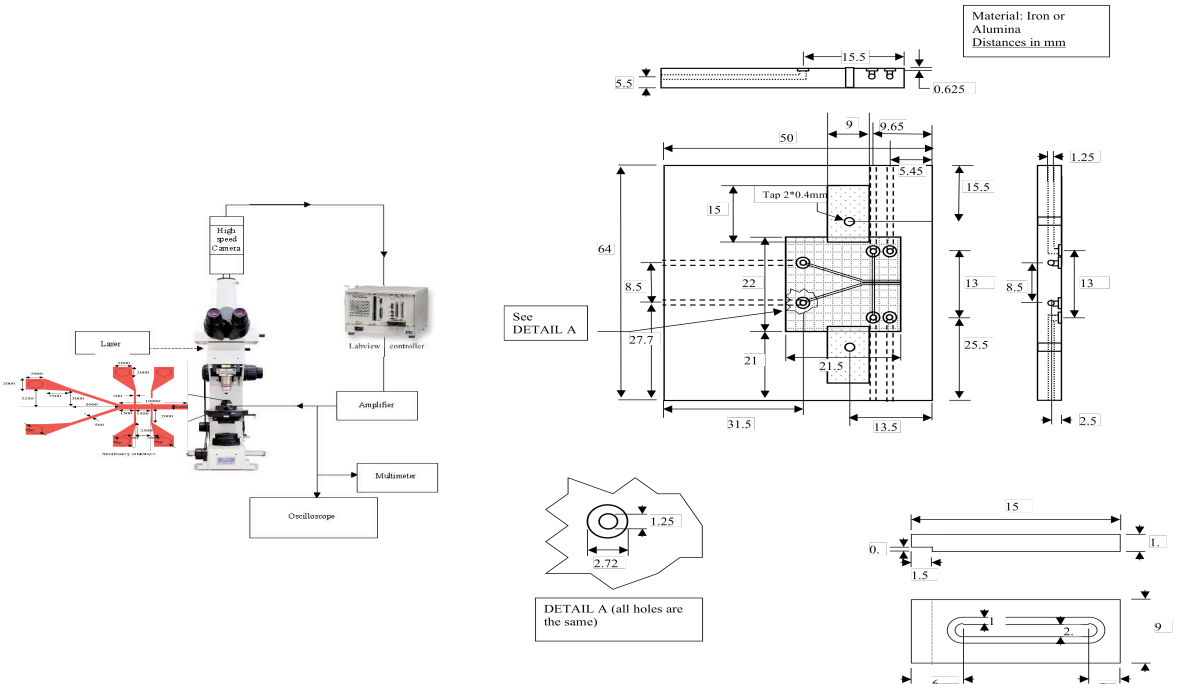

Figure 2: Design of the Synthetic Turbulence Generator.

In figure 3 we show the assembled Synthetic Turblence Generator positioned on the stage. Intake holes are visible on the sides and at inlets to the main channel.

Experiments using the Synthetic Turbulence Generator

The theoretical studies we did (see below) highlighted that issues of combustion instability and robustness of flame can be overcome by using a linear array architecture for microcombustors. While the array was stable to failure of some of the microcombustors, it still required stable operation of a subset

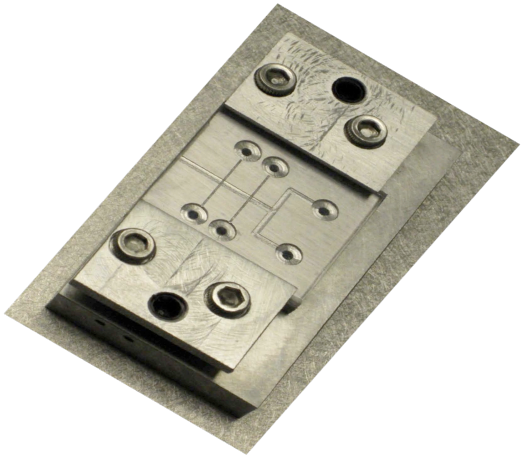

Figure 3: Assembled Synthetic Turbulence Generator (no cover).

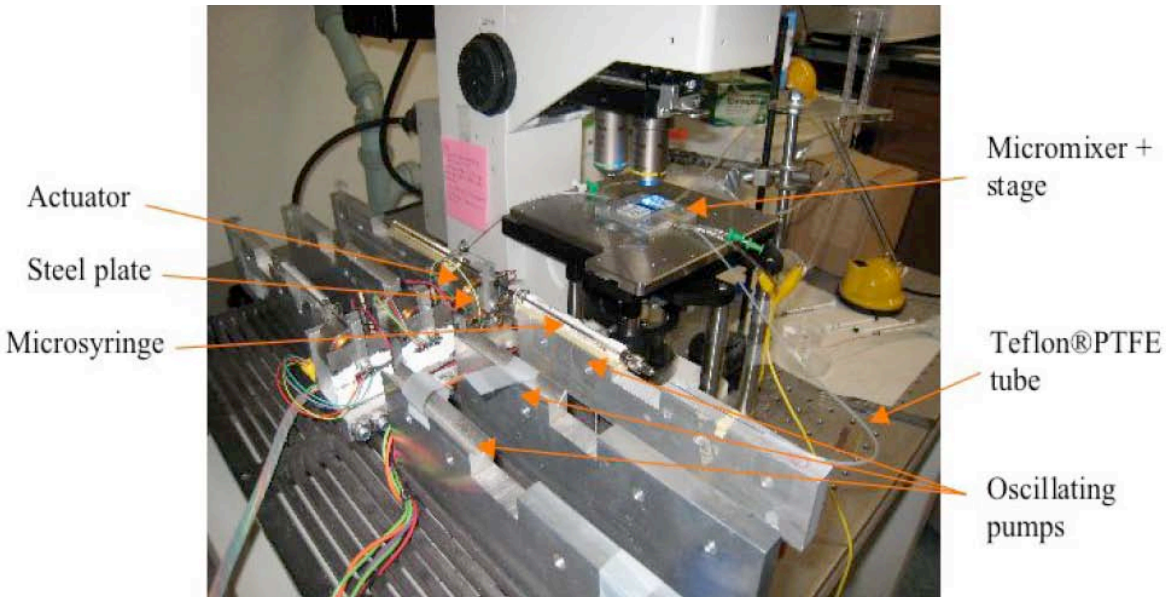

Figure 4: Experimental stage for mixing experiments.

of combustors. This stable operation depends on robustness of mixture coming into a microcombustor. We performed experiments to show improvement of mixing necessary for deployment of an array of combustors as described in the previous section. In figure 4 we show the experimental arrangement for mixing experiments. The mixer described in section 3 was actuated by linear displacement actuators seen in figure 4. Smoke was observed by the diffusion of a laser beam (Melles Griot HeNe) with a

neutral filter. The laser beam is pointed in the main channel through the outlet and carefully aligned with the canal to avoid reflexion on the walls and minimize background signal. Images are recorded via an Hamamatsu Orca camera and processed with Matlab. The observed results show the ability of the micromixer to distribute (premix) air and incoming fuel across the width of the microchannel, when parameters of side channel oscillation are optimized.

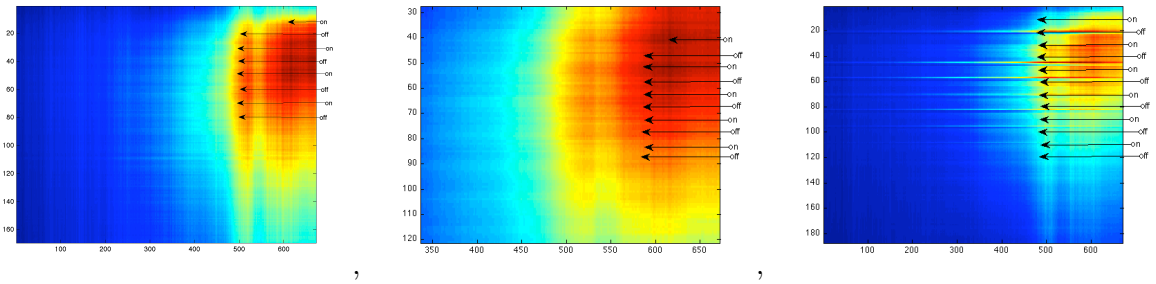

Figure 5: Smoke distribution in the center of the channel. Each line is the Smoke is injected on the right, air on the left. Mixing is turned on and off to observe the evolution of the air-smoke interface. Mixing parameters : amplitude 120 μm, frequency 184Hz. Left, first side channels off, second side channel on, center, first side channel is on, second is off, right, both sides channels are on with 180 phase.

1.2 Modelling of Combustion in a Single Channel

The combustion of premixed methane flame can be described using simple heat and mass transport equations. In the case of a thin rectangular channel, combustion can be modeled by 1D equations.

Non-dimensional equations in 1D

For a plane flame moving along the x-axis in the channel with temperature $\theta(x)$, we can use a 1D thermo-diffusive model with constant thermo-physical properties and single-step chemistry [4]:

$$\begin{cases} \frac{\partial T}{\partial t} &= \frac{\partial^2 T}{\partial x^2} - V\frac{\partial T}{\partial x} + (1-\sigma)W(c,T) - \Omega(T-\theta), \\ \frac{\partial c}{\partial t} &= \frac{1}{Le}\frac{\partial^2 c}{\partial x^2} - V\frac{\partial c}{\partial x} - W(c,T). \end{cases} \tag{1}$$

Here T is the scaled gas temperature in units of T_b, the adiabatic temperature of combustion; θ is the temperature of the channel wall in units of T_b; c is the scaled concentration of premixed reactant in units of c_0 (value in the fresh mixture); x is the scaled spatial coordinate in units of l_{th}, the thermal width of flame; V is the gas velocity in units of U_b, the adiabatic flame velocity; Le is the Lewis number; Ω is the heat exchange parameter; σ is the scaled temperature of the fresh mixture.

The rate of a one-step chemical reaction is described by the Arrhenius law. $W(c,t)$ is the non-dimensional rate of volumetric chemical reaction:

$$W(c,T) = \frac{1}{2}N^2(1-\sigma)^2 c \exp\left(N\left(1-\frac{1}{T}\right)\right), \tag{2}$$

where N is the non-dimensional activation energy.

The boundary conditions are defined as:

$$\begin{cases} c = 1, & T = \sigma & \text{at } x = +L \\ c = 0, & \frac{\partial T}{\partial x} = 0 & \text{at } x = -L \end{cases} \tag{3}$$

where L is the length of the channel. The gas entering at $x = +L$, is advected to the left with velocity V and exits the tube at $x = 0$.

It is first assumed that the tube is heated by an external heat source to temperature Θ and is approximated by the formula:

$$\theta(x) = \begin{cases} \sigma + (\Theta - \sigma)\exp(-\eta x), & \text{for } x > 0 \\ \Theta, & \text{for } x \leq 0 \end{cases} \tag{4}$$

Here η is the nondimensional characteristic length of the temperature drop in the tube wall.

When the wall is heated only by combustion, $\theta(x)$ can be found from the following equation:

$$\frac{\partial \theta}{\partial t} = K_w \frac{\partial^2 \theta}{\partial x^2} - \Omega_w(\theta - \sigma), \tag{5}$$

where K_w is the nondimensional thermal diffusion of the wall and Ω_w is the nondimensional heat exchange parameter. At $x = 0$, the gas flowing out of the combustion channel is acting as a heat source for the wall. This is described by the boundary condition:

$$\frac{\partial \theta}{\partial x} = -\eta(T - \sigma). \tag{6}$$

We also define a flame front coordinate X_f by the point corresponding to a maximum of chemical reaction rate W.

Initial external heating phase

We simulate reaction first using externally heated wall condition which is modelled using Eq. 4. During the initial external heating phase, the front can behave differently depending on operating conditions. It can stay stationary at a fixed location or show oscillatory motions (with or without extinction-ignition cycles). We numerically solved the system of partial differential equations using finite element software Comsol with $\Omega = 0.627$, $\eta = 0.059$, $\sigma = 0.2$, $N = 10$, $Le = 0.9$. In the phase diagram shown in Fig. 6, three of the trajectories are represented by dots. In those cases and at steady state, the flame front stays at the same position at all time. The trajectory plotted in green shows an oscillatory motion of the flame front with small amplitude. The two trajectories in blue show oscillations with alternating small and high amplitudes. The trajectory in red shows high-amplitude oscillations of the flame front with the flame periodically exiting the tube ($X_f < 0$).

There are two qualitatively different types of flame front oscillations: one with extinction-ignition cycles where the reaction rate at the flame front has periodically very low values (extinction) followed by high values (re-ignition); and another one with no extinction. This can be seen more precisely in Fig. 6 where the time dependence of the reaction rate at the flame front is plotted for three different values of (Θ, V). During the extinction-ignition oscillations, extinction happens when the flame fronts get the closest to the tube exit, $x = 0$ (or outside of the tube, $x < 0$). To better understand the

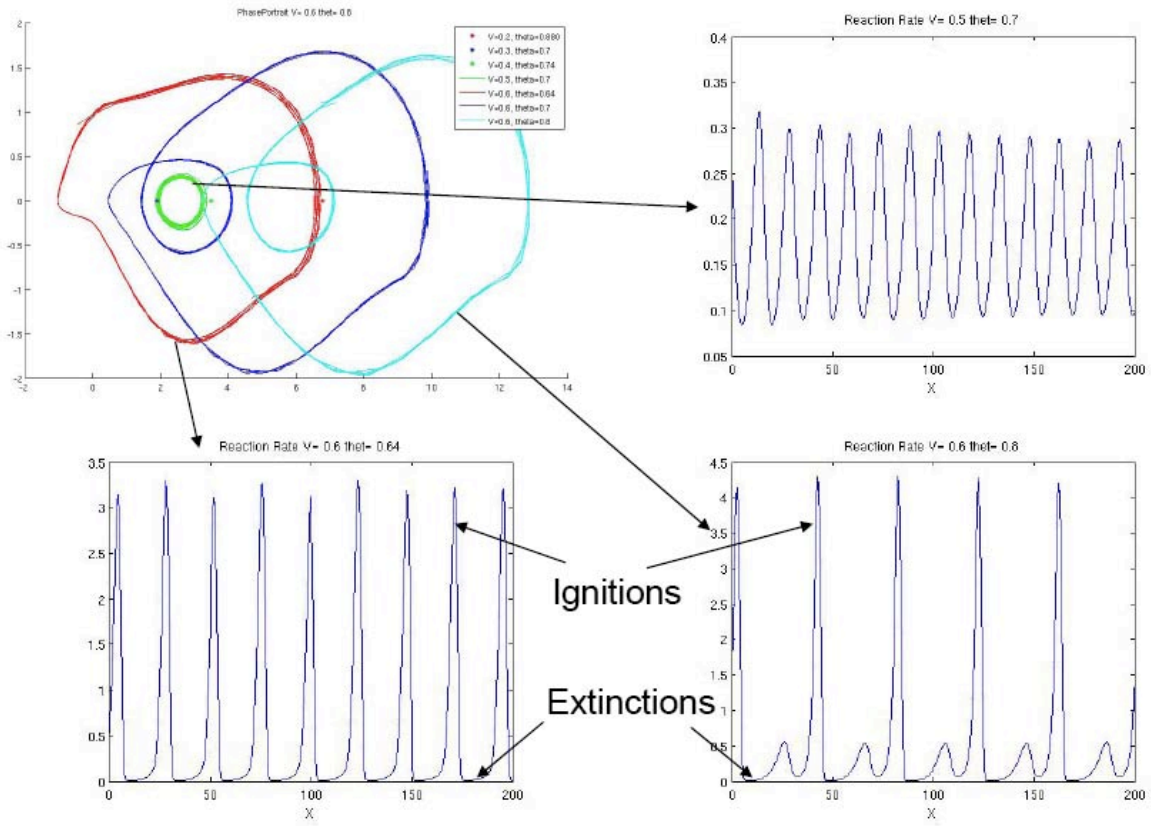

Figure 6: Reaction rate at flame front with external heating for different values of V and Θ. The flame front phase diagram $(X_f, \dot{X}_f)$ is shown on the top left. Position of the flame front with respect to time is shown for three different operating conditions.

influence of the gas velocity V and the external wall temperature Θ, we numerically solved the system of equations for values of V and Θ on a grid with $V = [0.1 : 0.05 : 0.6]$ and $\Theta = [0.6 : 0.02 : 0.9]$. In Fig. 7, top left panel shows the value of flame front temperature; the top right panel shows the value of flame front position; the bottom left panel shows the flame front reaction rate; and the bottom right panel is the max amplitude of oscillations. As the gas velocity and the wall heating increase, the flame front moves closer to the inlet ($x = L$). For gas velocity between 0.1 and 0.45, there is no oscillations. For higher gas velocities oscillations start to appear. The mean reaction rate increases with velocity but for high velocity repetitive extinction-ignition cycles appear (minimum value of the reaction rate is small).

Combustion in single microchannel with no external heating phase

All of the observations in the previous section were done for the case where external heating helps support the combustion throughout the simulation period. Now we describe simulations in which, after the wall temperature reaches a stationary solution, we remove the external heating and the wall is heated only by the combustion as modelled by Eq. 5. If the system temperature after phase 1

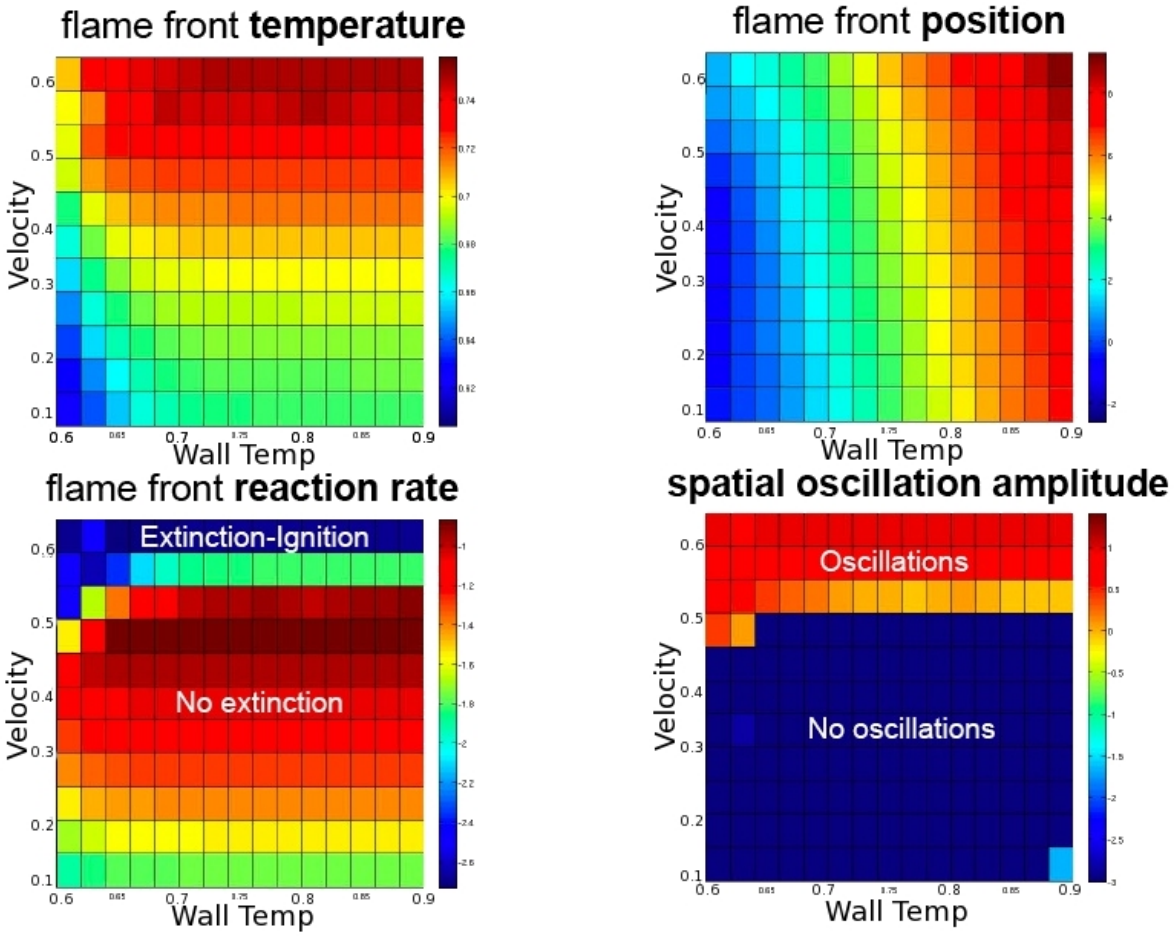

Figure 7: Values of temperature, position, reaction rates and spatial oscillation ampitude for different values of (Θ, V).

is high enough, the system converges to a solution independent of the initial heating. If the system temperature after external heating is too low (T=0.6 for our simulation parameters), we observe quenching of the flame front (Fig. 8). In that case, the heat loss through the wall is greater than the heat gained from the methane combustion. In the next section we show that problems with oscillation and high ignition temperature can be resolved using an array of microchannels instead of a single channel.

1.3 Modelling of Combustion in an Array of Channels

We are interested here in the coupling effect of an array of 3 or 5 channels and the effect of the distance between channels, d on the presence of self-sustained combustion starting from the low ignition temperature $T = 0.6$.

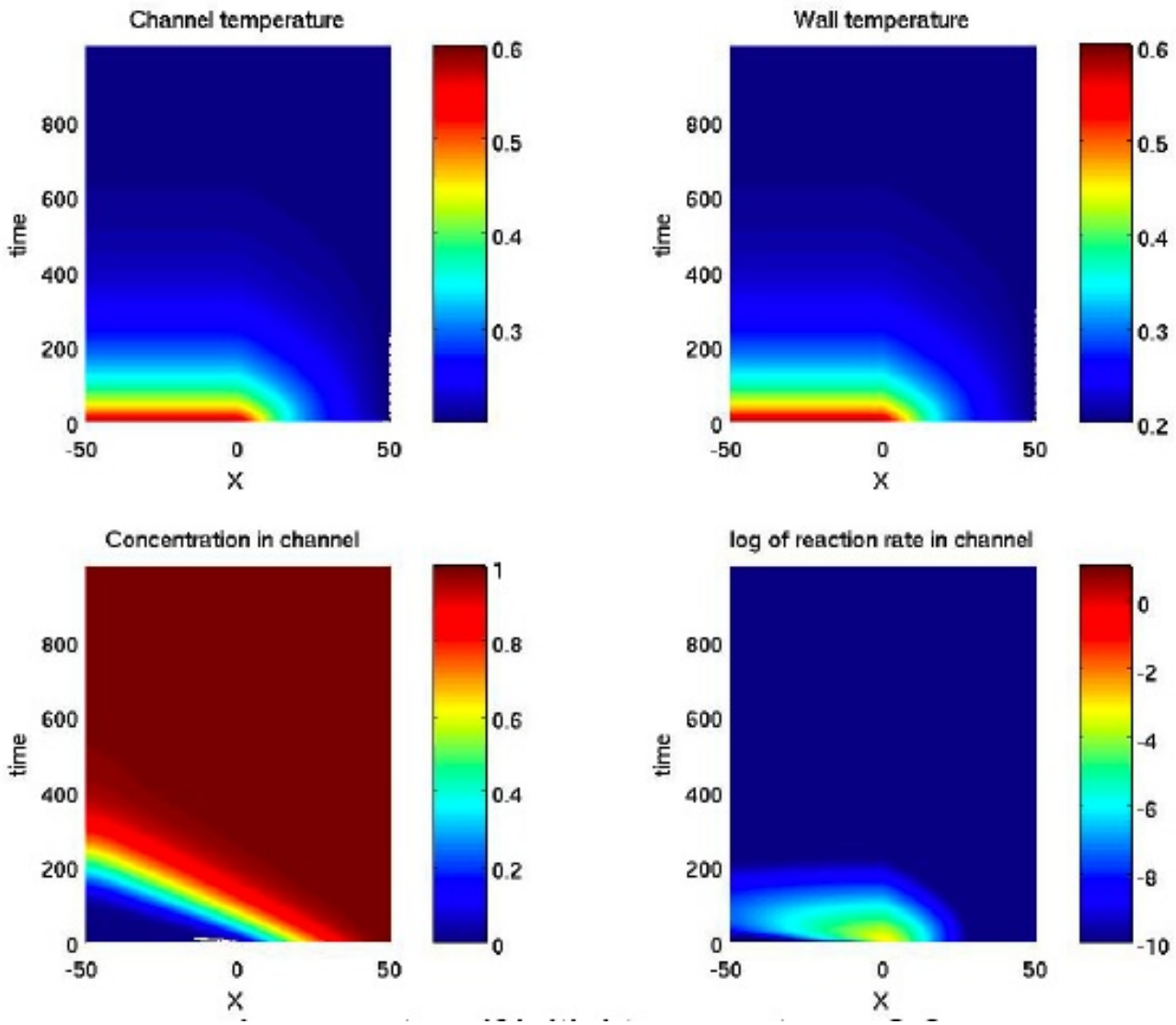

Figure 8: Temporal and spatial variation of wall temperature, gas concentration and reaction rate for ignition temperature $T = 0.6$.

Model

Each channel is modelled by a system of three equations similar to the one presented in the previous section. Let i be the index of the channel.

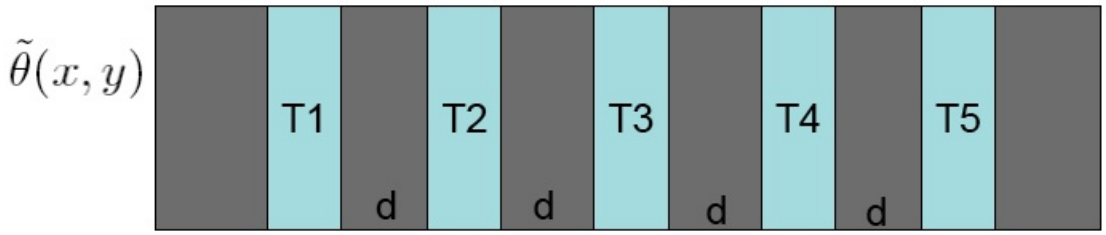

Figure 9: An array of 5 microchannels separated by distance d from each other.

Inside the channels, $(x \geq 0)$, we solve the following system of equations:

$$\begin{cases} \frac{\partial T_i}{\partial t} &= \frac{\partial^2 T_i}{\partial x^2} - V\frac{\partial T_i}{\partial x} + (1-\sigma)W(c_i,T_i) - \Omega(T_i - \tilde{\theta}(x,(i-1)d)), \\ \frac{\partial c_i}{\partial t} &= \frac{1}{Le}\frac{\partial^2 c_i}{\partial x^2} - V\frac{\partial c_i}{\partial x} - W(c_i,T_i), \\ \frac{\partial \theta_i}{\partial t} &= K_w\frac{\partial^2 \theta_i}{\partial x^2} - \Omega_w(\theta_i - \sigma). \end{cases} \tag{7}$$

Outside the channels, $(x < 0)$, we solve the following system of equations:

$$\begin{cases} \frac{\partial T_i}{\partial t} &= \frac{\partial^2 T_i}{\partial x^2} - V\frac{\partial T_i}{\partial x} + (1-\sigma)W(c_i,T_i), \\ \frac{\partial c_i}{\partial t} &= \frac{1}{Le}\frac{\partial^2 c_i}{\partial x^2} - V\frac{\partial c_i}{\partial x} - W(c_i,T_i), \\ \frac{\partial \theta_i}{\partial t} &= K_w\frac{\partial^2 \theta_i}{\partial x^2} - \Omega_w(\theta_i - \tilde{T}_i). \end{cases} \tag{8}$$

Channel i located at $y = (i-1)d$ is at temperature $T_i(x)$ and is bounded by two walls at temperatures given by $\tilde{\theta}(x,y)$. In the direction tangential to the channels (y-direction), the heat dissipates inside the wall material which is in contact with room temperature σ. For each x, the temperature in the y-direction, $\tilde{\theta}(y)$, follows the equation:

$$K_w\frac{\partial^2 \tilde{\theta}}{\partial y^2} - \Omega_w(\tilde{\theta} - \sigma) = 0. \tag{9}$$

We assume that the temperature profile in the y-direction is achieved instantly. At the location of the channels ($y = 0$, $y = d$, $\cdots$, $y = 4d$) the gas heats the wall along the channel with the heat flux:

$$\frac{\partial}{\partial y}\tilde{\theta}(y = (i-1)d^-) + \frac{\partial}{\partial y}\tilde{\theta}(y = (i-1)d^+) = 2\eta(\theta_i(x) - \sigma) \tag{10}$$

The temperature $\tilde{\theta}(y)$ is continuous at the location of the channels but its derivative is not. The notations $\frac{\partial}{\partial y}\tilde{\theta}(y = (i-1)d^-)$ and $\frac{\partial}{\partial y}\tilde{\theta}(y = (i-1)d^+)$ represent the value of the derivative on the left side and right side of channel i. The expression $\theta_i(x)$ is asolution of the 1D heat equation along the wall of a channel:

$$\frac{\partial \theta_i}{\partial t} = K_w\frac{\partial^2 \theta_i}{\partial x^2} - \Omega_w(\theta_i - \sigma) \tag{11}$$

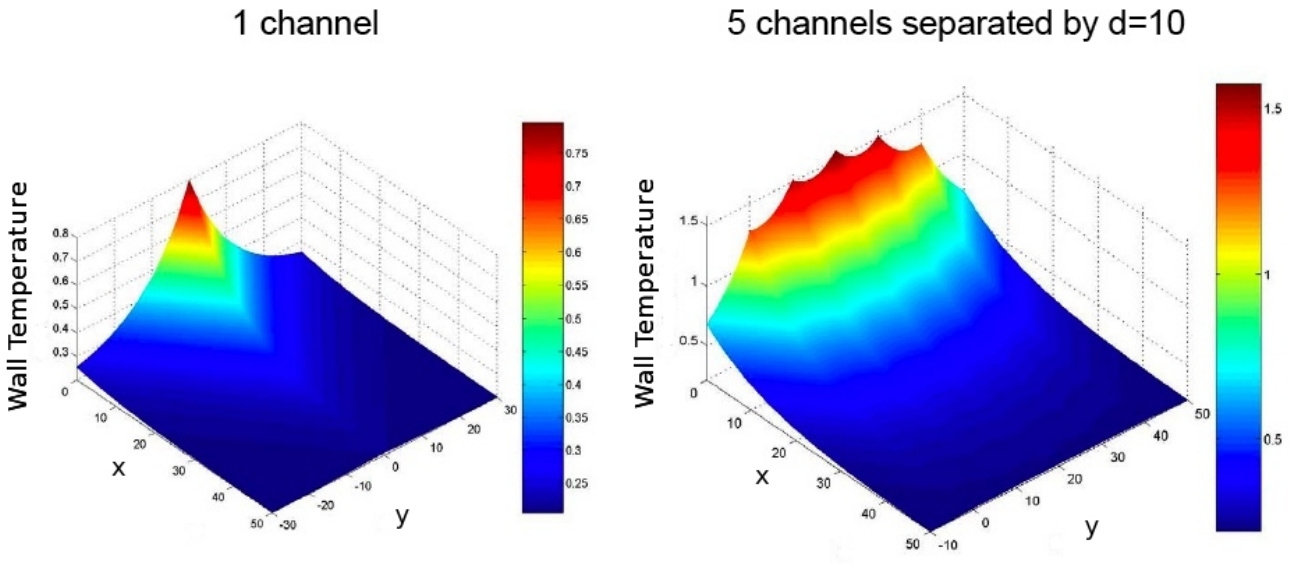

Figure 10: Array wall temperature $\tilde{\theta}(x, y)$ for a single channel and an array of 5 channels.

with boundary conditions:

$$\begin{cases} \frac{\partial \theta_i}{\partial x} = -\eta(\tilde{T}_i - \sigma) & \text{at } x = 0 \\ \theta_i = \sigma & \text{at } x = L \end{cases} \tag{12}$$

Single-channel exit temperature $\tilde{T}_i$ in Eqs. 8 and 12 are expressed through array channel temperatures $T_i(0)$ via a transformation inverse to the one from single-channel wall temperatures $\theta_i(x)$ to array temperatures $\tilde{\theta}(x, (i-1)d)$.

We analytically solved the equation for the wall temperature in the y-direction. The temperature T_i is a combination of the neighboring channel gas temperatures (see Fig. 10). The wall temperatures in an array of nearby channels are significantly higher.

Self-Sustained Combustion

The combustion stability in an array containing 3 microchannels and 5 microchannels for different inlet gas velocities and distances between microchannels is shown in Fig. 11. For each channel a dot is plotted in a different color corresponding to the combustion steady state in that channel. If the steady state corresponds to the flame extinction, the dot is red. If the flame is stable at a fixed location, the dot is green. If the location of the flame is oscillatory, the dot is blue. With ignition temperature of 0.6, combustion cannot be sustained in a single channel (for any gas velocity). In an array of channels, for a wide range of velocities and distances between channels, we can obtain stationary combustion (green) and oscillatory combustion (blue) in all channels. As distance between channels increases, channels get less heating from their neighbours and the solution becomes identical to the case of a single channel with no combustion (red).

It is evident from these results that deploying an array of channels instead of a single microchannel prevents onset of combustion instability and provides robustness of operation over a range of param-

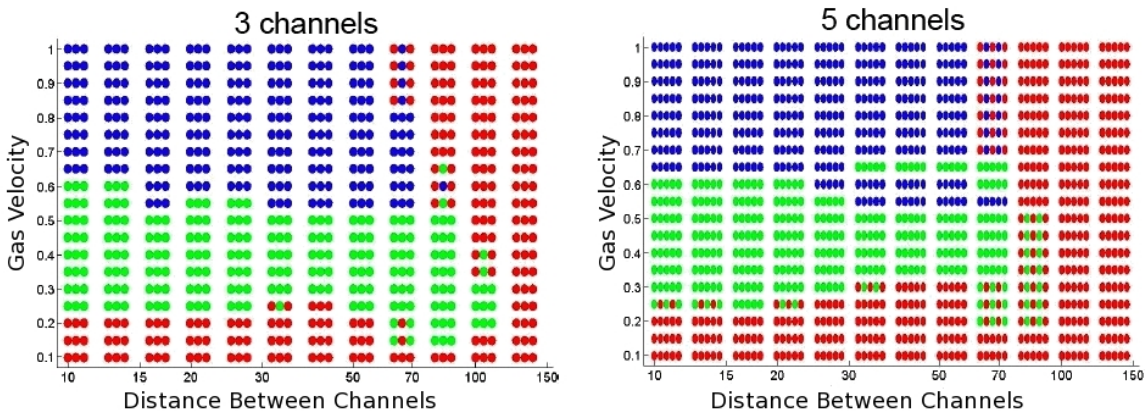

Figure 11: Combustion stability in an array containing 3 microchannels (left) and 5 microchannels (right) for different inlet gas velocities and distances beween microchannels.

eters, thus showing that linear array architecture could be utilized effectively to achieve the goals of micropower generation.

2 Personnel supported:

Dr. Igor Mezić , Dr. Maud Mader, Dr. Frederic Bottausci, Dr. Sophie Loire, Dr. Vladimir Fonoberov

3 Interactions/transitions:

We had a strong interaction with the laboratory of Professor Nick Glumac at the Mechanical and Industrial Engineering Department of the University of Illinois, Urbana-Champaign in whose machine shop the Synthetic Turbulence Generator was produced.

References

[1] F. Bottausci, C. Cardonne, C. Meinhart, and I. Mezić. An ultrashort mixing length micromixer: The shear superposition micromixer. *Lab on a Chip*, 7(3):396–398, 2007.

[2] F. Bottausci, I. Mezić, C.D. Meinhart, and C. Cardonne. Mixing in the shear superposition micromixer: three-dimensional analysis. *Philosophical Transactions A*, 362(1818):1001, 2004.

[3] S. Loire, I. Mezić, and V. Fonoberov. Combustion of methane in microchannels . *Proceedings of the ASME 2009 International Mechanical Engineering Congress & Exposition November 13-November 19, 2009, Lake Buena Vista, Fl, USA*.

[4] S. Minaev, K. Maruta, and R. Fursenko. Nonlinear dynamics of flame in a narrow channel with a temperature gradient. *Combustion Theory and Modelling*, 11:1364–7830, 2007.